NASA TECHNICAL NOTE

NASA TN D-7224

NASA TN D-7224

ELECTRON AVALANCHE STRUCTURE DETERMINED BY RANDOM WALK THEORY

by Gerald W. Englert

Lewis Research Center
Cleveland, Ohio 44135

NATIONAL AERONAUTICS AND SPACE ADMINISTRATION • WASHINGTON, D. C. • APRIL 1973

1. Report No.	2. Government Accession No.	3. Recipient's Catalog No.
NASA TN D-7224		

4. Title and Subtitle	5. Report Date
ELECTRON AVALANCHE STRUCTURE DETERMINED BY RANDOM WALK THEORY	April 1973
	6. Performing Organization Code
7. Author(s)	8. Performing Organization Report No.
Gerald W. Englert	E-7074
	10. Work Unit No.
9. Performing Organization Name and Address	503-10
Lewis Research Center National Aeronautics and Space Administration Cleveland, Ohio 44135	11. Contract or Grant No.
	13. Type of Report and Period Covered
12. Sponsoring Agency Name and Address	Technical Note
National Aeronautics and Space Administration Washington, D.C. 20546	14. Sponsoring Agency Code

15. Supplementary Notes

16. Abstract

A self-consistent avalanche solution which accounts for collective long range Coulomb interactions as well as short range elastic and inelastic collisions between electrons and background atoms is made possible by a random walk technique. Results show that the electric field patterns in the early formation stages of avalanches in helium are close to those obtained from theory based on constant transport coefficients. Regions of maximum and minimum induced electrostatic potential φ are located on the axis of symmetry and within the volume covered by the electron swarm. As formation time continues, however, the region of minimum φ moves to slightly higher radii and the electric field between the extrema becomes somewhat erratic. In the intermediate formation periods the avalanche growth is slightly retarded by the high concentration of ions in the tail which oppose the external electric field. Eventually the formation of ions and electrons in the localized regions of high field strength more than offset this effect causing a very abrupt increase in avalanche growth.

17. Key Words (Suggested by Author(s))	18. Distribution Statement
Electron avalanche Gaseous breakdown Random walk Transport coefficients	Unclassified - unlimited

19. Security Classif. (of this report)	20. Security Classif. (of this page)	21. No. of Pages	22. Price*
Unclassified	Unclassified	41	$3.00

* For sale by the National Technical Information Service, Springfield, Virginia 22151

ELECTRON AVALANCHE STRUCTURE DETERMINED BY RANDOM WALK THEORY

by Gerald W. Englert

Lewis Research Center

SUMMARY

The early stages of a large number of avalanche formations in helium were determined by means of computer simulation of the microscopic details. The exact trajectory of each electron was followed as it experienced various types of collisions with the background atoms and as it was acted upon by the electric field in the time between collisions. Results of such a lengthy procedure show that the electron transport coefficients of avalanches in helium relax to local equilibrium values in approximately one-hundredth of the formation time of a fully developed avalanche. This enables the use of a random walk concept for avalanche study in which the step sizes and probabilities are based on electron transport coefficients; these coefficients depending only on the background density and the local electric field strengths within the avalanche. This repetitious procedure permits a self-consistent avalanche solution which accounts for collective long range Coulomb interactions as well as short range elastic and inelastic collisions with a reasonable expenditure of computer time.

The electric field patterns initially formed inside the avalanches were close to those obtained from theory based on constant transport coefficients. A region of maximum and one of minimum induced electrostatic potential φ were located on the axis, and within the volume covered by the electron swarm. As formation time continues, the region of minimum φ moves to slightly higher radii. The electric field in the axial distance between the two extrema builds up and diminishes in a somewhat erratic manner.

In the intermediate time periods the avalanche growth is slightly retarded by the high concentration of ions in the tail which oppose the external electric field. Eventually, at a value of the time-pressure parameter tp slightly greater than 3.9×10^{-4} sec-N/m^2 (2.9 μsec torr) the formation of ions and electrons in the regions of high field strength more than offset this effect, causing a very abrupt increase in avalanche growth. It is assumed that the internal electric field is axisymmetric. The random walk calculations were not carried much beyond the onset of the rapid growth period since assuming axisymmetry is not justified there.

INTRODUCTION

The subject of this report is the formation of an electron avalanche, in an electric field, independent of wall effects (secondary ionization). This process is initially quite orderly, starting with one electron and continuing with an exponential growth of free electrons as a result of ionizing collisions between these electrons and the background gas. Such avalanches are descriptive of those which, for example, form at discrete locations throughout the volume of a gas, the gas undergoing initial ionization to form a plasma. If the formation of any single avalanche is continued under suitable conditions until sufficiently strong internal electric fields are built up, a local needle-like ionization pattern (streamer) is abruptly formed (ref. 1). This can ultimately result in a turbulent sparking process. This latter process is beyond the range of application of the techniques employed in the present investigation. A fully developed avalanche will be defined herein as one which has grown to the streamer formation stage.

Changes occur in avalanche formations in such short time periods that even the external characteristics are difficult to measure. Theoretical solution is difficult since the descriptive differential equations are very nonlinear due to the extreme spatial and timewise changes of the internal electric fields. A means of investigating various theoretical models of internal structure which allows incorporation of considerable physical detail could be quite useful.

Random walk theory was employed in the computer simulation of the microscopic details of electron motion in references 2 and 3. This theory includes both elastic and inelastic short range collisions between the electrons and background neutrals, and permits an exact calculation of the electron trajectory between such events. Since more than 10^8 ionizations usually occur in the development of an avalanche up to the streamer formation stage, computer time expenditure becomes a serious problem when each electron is walked in detail.

Where a large number of microscopic events occurs within small macroscopic volume elements and time increments, the step sizes and probabilities used in the random walk (RW) can be based on local averages. This in turn greatly facilitates the calculation procedure. It was demonstrated in references 4 and 5 that such a technique can be used to simulate a pertinent class of parabolic nonlinear differential equations. This type of RW was suggested in reference 6 as a means of solution of the electron transport equation. The step sizes and probabilities are determined in terms of the coefficients of the transport equation which, in turn, are dependent only on the local electric field and background density.

In avalanche formations, the density of charged particles can reach values such that long range Coulomb interactions (thus internal, i.e., induced, electric fields) must be considered as well as the short range interactions between the free electrons and

background gas particles. Application of the RW technique of references 4 and 5 to the electron avalanche in a manner which preserves microscopic influence, yields a self-consistent internal electric field, and yet enables a solution with a reasonable amount of computer time was undertaken. Numerical results were obtained for avalanche formations in helium at a ratio of external electric field to background pressure of 22.5 V-m/N (30 V/cm-torr).

ANALYSIS

Microscopic Random Walk

In principle, the electron motion in an avalanche can be precisely simulated by random walks. The trajectory of each electron is followed as it undergoes various types of collisions and as it is acted upon by the electric field in the time between collisions. The details of each collision are based on random selection of values from sets of numbers distributed in accordance with cross section data. This is essentially the procedure of references 2 and 3. In these references, a constant number (representative sample) of electrons were followed to study a process having a uniform density of electrons. In the present study, however, an additional electron (therefore, walk) originates at each ionizing collision, and spatial effects are of prime concern.

Such a RW procedure provides an excellent means for computer simulation of microscopic details of avalanche formation. It requires a large amount of computer time, however, due to the exponential buildup of electrons. This method is feasible in the early stages of avalanche formation ($N \leq 10^4$ electrons). With this number of electrons and/or ions the internal electric field is negligible and only interactions of the electrons with the background atoms need be considered.

This procedure was applied to the formation of a large number of electron avalanches in helium. The location of the electrons and ions, at various times from the start of the buildup, is shown in the computer plots of figure 1. All charged particle locations are shown here as if looking through a side view of the avalanche. That is, the charged particle locations are projected along lines perpendicular to the paper, which represents a plane through the x and z axes of the coordinate system. The origin of the coordinate system is the starting point ($t = 0$) of the trajectory of the first electron. The external electric field is in the negative z direction.

The electrons essentially move in a spherical swarm. The ion pattern is that expected from cloud chamber photographs (ref. 7).

These avalanches were started with a number of electrons N_0 considerably greater than one to get a higher density of points and a better definition of shape during the low formation times shown. The plots can also be considered to represent a superposition

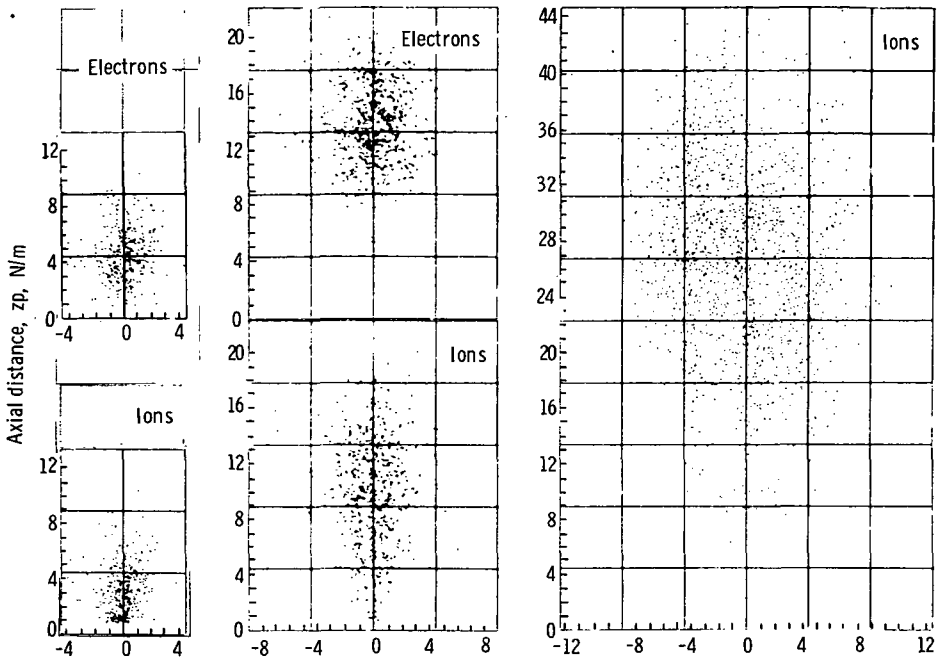

(a) Avalanche formation time tp = 1.3×10^{-5} sec-N/m^2; number of superimposed avalanches N_0 = 300; number of ionizations N = 301.

(b) Avalanche formation times tp = 4.5×10^{-5} sec-N/m^2; number of superimposed avalanches N_0 = 145; number of ionizations N = 1311.

(c) Avalanche formation time tp = 9.1×10^{-5} sec-N/m^2; number of superimposed avalanches N_0 = 11; number of ionizations N = 1739.

Figure 1. - Particle locations obtained by use of microscopic RW procedure at three avalanche formation times. Electric field parameter E/p = 22.5 V-m/N; initial energy of first electron of N_0 avalanches is uniformly distributed from 0 to 12 eV.

of N_0 avalanches, each starting with one electron, thus giving a representative average of formation patterns when the number of charged particles per avalanche is low.

The electron transport coefficients were also determined in these computations, and are given in figures 2 and 3. Relaxation to terminal steady-state conditions were found to occur in short generalized time periods, tp, close to those found in reference 2, which is about one-hundredth of the formation time of a fully developed avalanche. Data scatter is due to the sample size. The number N_0 of superimposed avalanches was selected so that there was a total of about 10^3 electrons when formation time reached relaxation time.

Approximately 10 minutes of computer time is required to determine formations having the order of 10^3 electrons. Avalanche structure on the order of 10^{-4} sec-N/m^2 range is of main interest. Then the number of electrons may reach the order of 10^{10} electrons. Use of the detailed RW would thus require far excessive amounts of computer time during such long time periods. This, however, is where the use of equilibrium values of transport coefficients is justified. The electron motion can then be described by the electron transport equation (appendix B). This equation describes the electron motion by diffusion

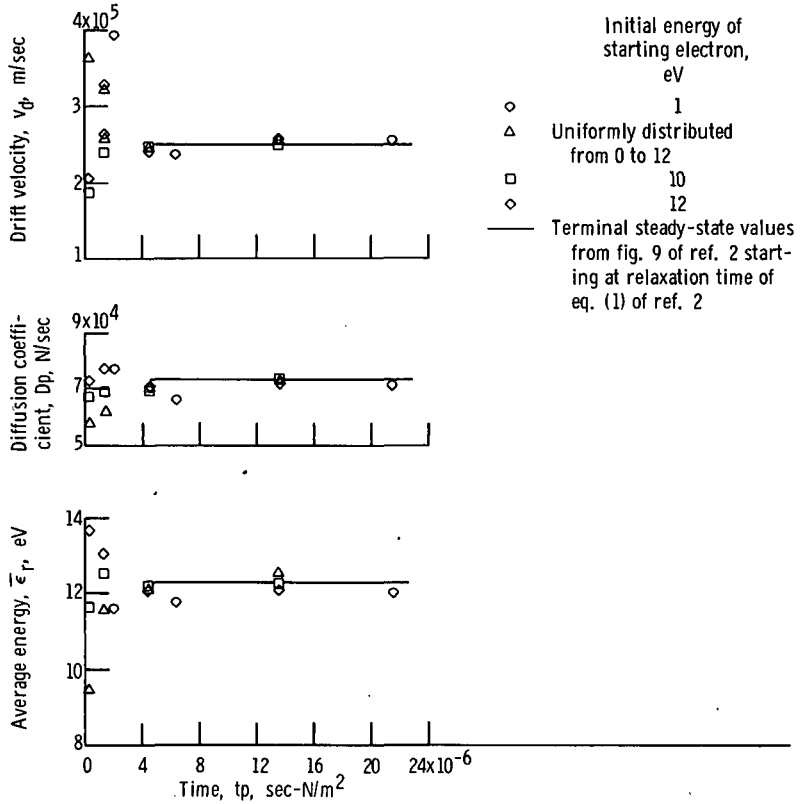

Figure 2. - Relaxation of electron drift, diffusion coefficient, and average energy. Electric field parameter E/p = 22.5 V-m/N.

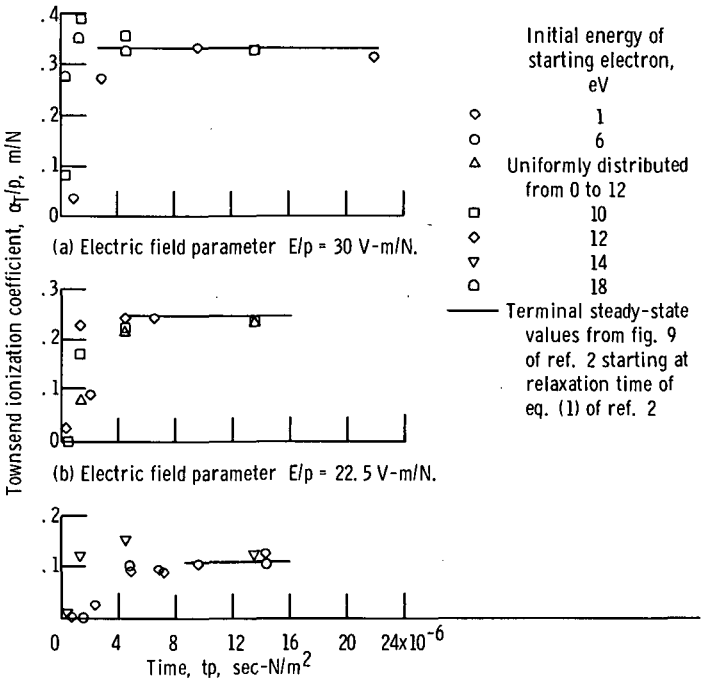

Figure 3. - Relaxation of ionization coefficient at three values of electric field parameter.

and drift expressions while accounting for ionization events by a source term.

The amount of avalanche buildup by the time that relaxation time is reached constitutes a very small fraction of the electron population in the later main time range of interest. The electron transport equation can thus be assumed to apply to avalanche formations from the start with negligible consequence.

Macroscopic Random Walk

Random walk theory. - The nonlinear parabolic form of the electron transport equation is similar to that of equations solved by the RW-on-a-grid concept in references 4 and 5. In this RW procedure the required step sizes and probabilities are expressed in terms of the coefficients of the partial differential equation to be solved.

The general equation describing a RW on a grid is (ref. 4)

$$\frac{\partial W}{\partial t} = \sum_{j=1}^{3} \left\{ - \frac{\partial \left[\left(P_j^+ - P_j^- \right) W \right]}{\partial X_j} \frac{\Delta X_j}{\Delta t} + \frac{1}{2} \frac{\partial^2 W}{\partial X_j^2} \frac{\left(\Delta X_j \right)^2}{\Delta t} \right\} \tag{1}$$

The symbols are defined in appendix A. This equation, based on the law of compound probability, is essentially a law of conservation of particles as they move to and from neighboring points on a three-dimensional lattice (fig. 4). The components of the step sizes ΔX_j are the grid spaces. The terms P_j^+ and P_j^- are the probabilities of taking steps in the positive and negative directions along the j^{th} coordinate. It is assumed that each of the three components of the steps contribute to the particle movement during each time increment Δt. Then

$$P_j^+ + P_j^- = 1 \qquad j = 1, 2, 3 \tag{2}$$

which corresponds to steps across diagonals of the lattice.

Let X_j where $j = 1, 2, 3$ be Cartesian coordinates. Then W, which is the probability density of particles being at a certain grid location at time t, can simply be set equal to the density of electrons n_e.

The components of step size ΔX_j are identifiable with second moments (root mean squared averages) of the components of the microscopic distance Δx_j between collisions. Letting a bar denote average,

$$\Delta X_j = \sqrt{\overline{\left(\Delta x_j \right)^2}} \qquad j = 1, 2, 3 \tag{3}$$

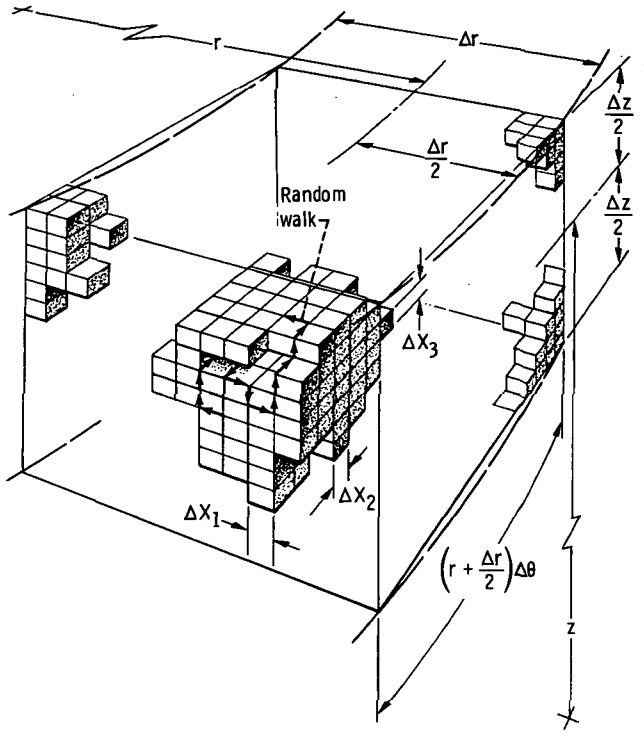

Figure 4. - Random walk on three-dimensional rectangular grid. Division of space into larger cylindrical zones for tallying purposes (appendix C) is shown by dashed lines. Radial distance r is measured from axis of avalanche. Axial distance z is measured from initial location of first electron.

Then using the definition of diffusion coefficient,

$$D_j = \frac{\overline{(\Delta x_j)^2}}{2\tau}$$

it follows that

$$\Delta X_j = \sqrt{2D_j\tau} \qquad j = 1, 2, 3 \tag{4}$$

The mean free time between collisions τ is equivalent to Δt. For helium, τ can be approximated by (ref. 2)

$$\tau = \frac{1}{(nQ_a v)} \tag{5}$$

This is because the product of electron velocity v with Q_a is very nearly constant over the range of interest herein. Here Q_a is the total absorption cross section for electrons colliding with neutral background (helium) atoms of density n. Setting v equal to $\sqrt{2\bar{\epsilon}/m}$, where $\bar{\epsilon}$ is the mean electron energy of reference 2 for the macroscopic RW, gives the very small variation of τ with E/p shown in figure 5.

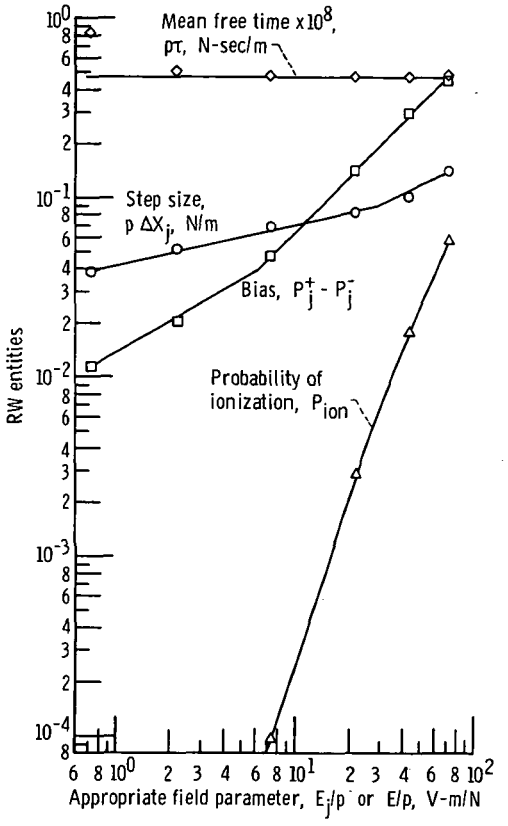

Figure 5. - Characteristic quantities of use in macroscopic RW. (Data points were calculated from transport coefficients of ref. 2; lines denote empirical curve fits used in the computer program.)

The bias $P_j^+ - P_j^-$ can be used to describe the influence of a preferred direction of (drift) velocity, which involves a first moment of Δx_j

$$P_j^+ - P_j^- = \frac{\Delta x_j}{\sqrt{\overline{(\Delta x_j)^2}}} = \frac{v_{d,j}\tau}{\sqrt{2D_j\tau}} \qquad j = 1, 2, 3 \tag{6}$$

Diffusion in the presence of an electric field has a nearly isotropic coefficient over the range of E/p of most concern in this investigation (see table I of ref. 2). It will be

assumed, therefore, that mean free time is constant and that step size is isotropic and only weakly dependent on space, although it can be strongly time dependent. Using equations (4) and (6) in (1) and identifying W with n_e then yields

$$\frac{\partial n_e}{\partial t} = - \nabla \cdot n_e \vec{v}_d + D \nabla^2 n_e \tag{7}$$

Consider ionizing events to occur during the RW with a probability per collision P_{ion}. The rate of ionizing events per unit volume is then $P_{ion} n_e / \tau$. This is equivalent to $\alpha_T v_d n_e$ where α_T is the Townsend first ionization coefficient. Thus

$$P_{ion} = \alpha_T v_d \tau$$

Equation (7), extended to include this source term, becomes

$$\frac{\partial n_e}{\partial t} = - \nabla \cdot n_e v_d + D \nabla^2 n_e + \alpha_T v_d n_e \tag{8}$$

This is equivalent to the electron transport equation (see appendix B) within the spatial restriction on step size (and thus on D for constant τ) which will be appraised further in the section entitled Results of Macroscopic RW. The transport equation can be written in terms independent of background density. To follow convention, however, pressure p referenced to 0° C will be used as

$$\frac{\partial n_e}{\partial (tp)} = \sum_{j=1}^{3} \left[- \frac{\partial n_e v_{d,j}}{\partial (X_j p)} + Dp \frac{\partial^2 n_e}{\partial (X_j p)^2} \right] + \frac{\alpha_T}{p} v_d n_e \tag{9}$$

Step size and probabilities are also plotted in figure 5. These values are based on the transport coefficients of reference 2.

Execution of the random walks. - In the execution of each step of the RW-on-a-grid procedure four numbers are drawn at random from a set of numbers uniformly distributed over the interval 0 to 1. Such sets of random numbers are available in most computer libraries. Three of these numbers are used to determine step direction. For example, if the j^{th} random number is less than the corresponding P_j^+, the component of

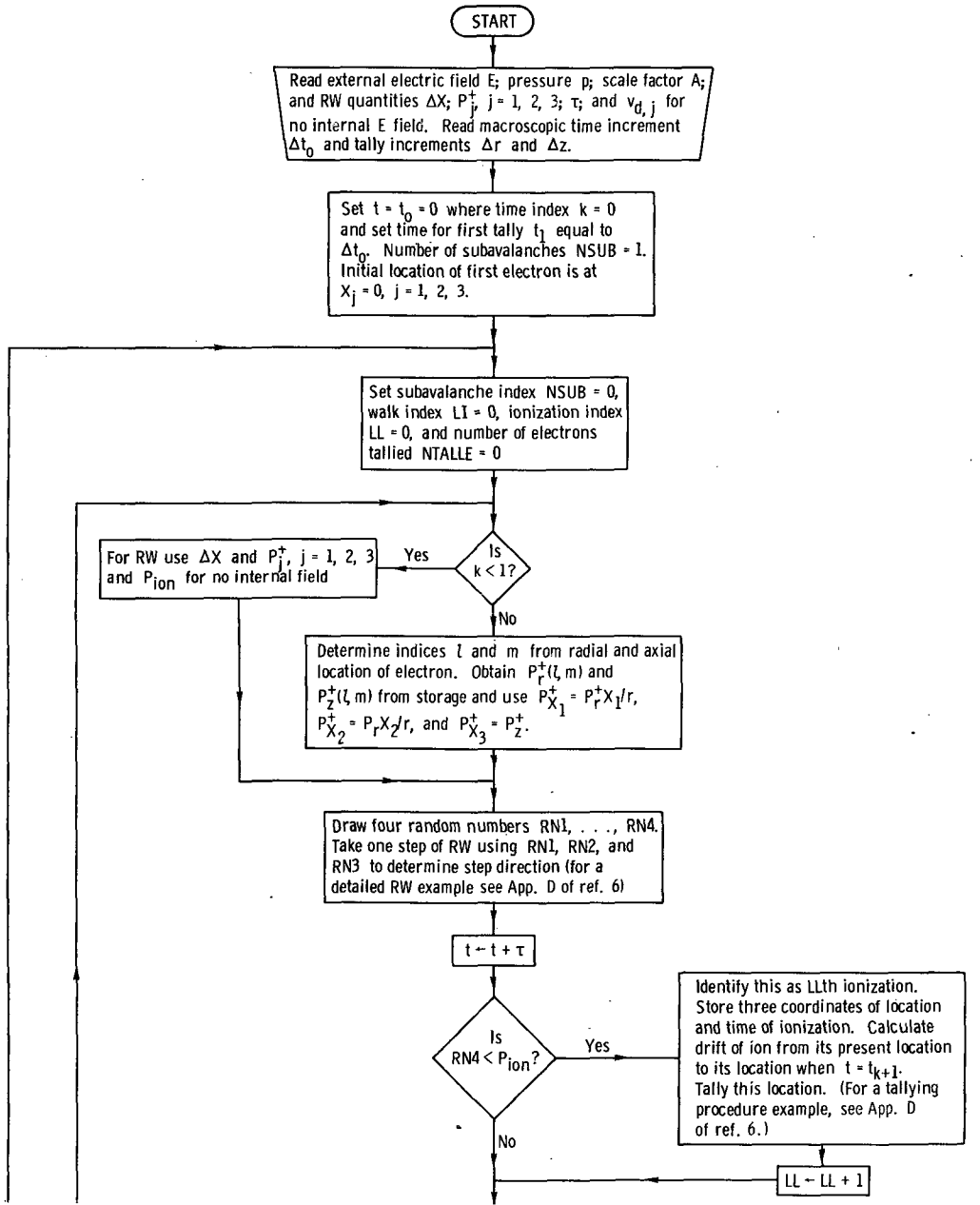
START
Read external electric field E; pressure p; scale factor A; and RW quantities ΔX; P_j^+, j = 1, 2, 3; τ; and $v_{d,j}$ for no internal E field. Read macroscopic time increment Δt_0 and tally increments Δr and Δz.
Set $t = t_0 = 0$ where time index k = 0 and set time for first tally t_1 equal to Δt_0. Number of subavalanches NSUB = 1. Initial location of first electron is at $X_j = 0$, j = 1, 2, 3.
Set subavalanche index NSUB = 0, walk index LI = 0, ionization index LL = 0, and number of electrons tallied NTALLE = 0
Is k < 1?
Yes
For RW use ΔX and P_j^+, j = 1, 2, 3 and P_{ion} for no internal field
No
Determine indices l and m from radial and axial location of electron. Obtain $P_r^+(l, m)$ and $P_z^+(l, m)$ from storage and use $P_{X_1}^+ = P_r^+ X_1/r$, $P_{X_2}^+ = P_r X_2/r$, and $P_{X_3}^+ = P_z^+$.
Draw four random numbers RN1, . . ., RN4. Take one step of RW using RN1, RN2, and RN3 to determine step direction (for a detailed RW example see App. D of ref. 6)
t ← t + τ
Is RN4 < P_{ion}?
Yes
Identify this as LLth ionization. Store three coordinates of location and time of ionization. Calculate drift of ion from its present location to its location when $t = t_{k+1}$. Tally this location. (For a tallying procedure example, see App. D of ref. 6.)
No
LL ← LL + 1

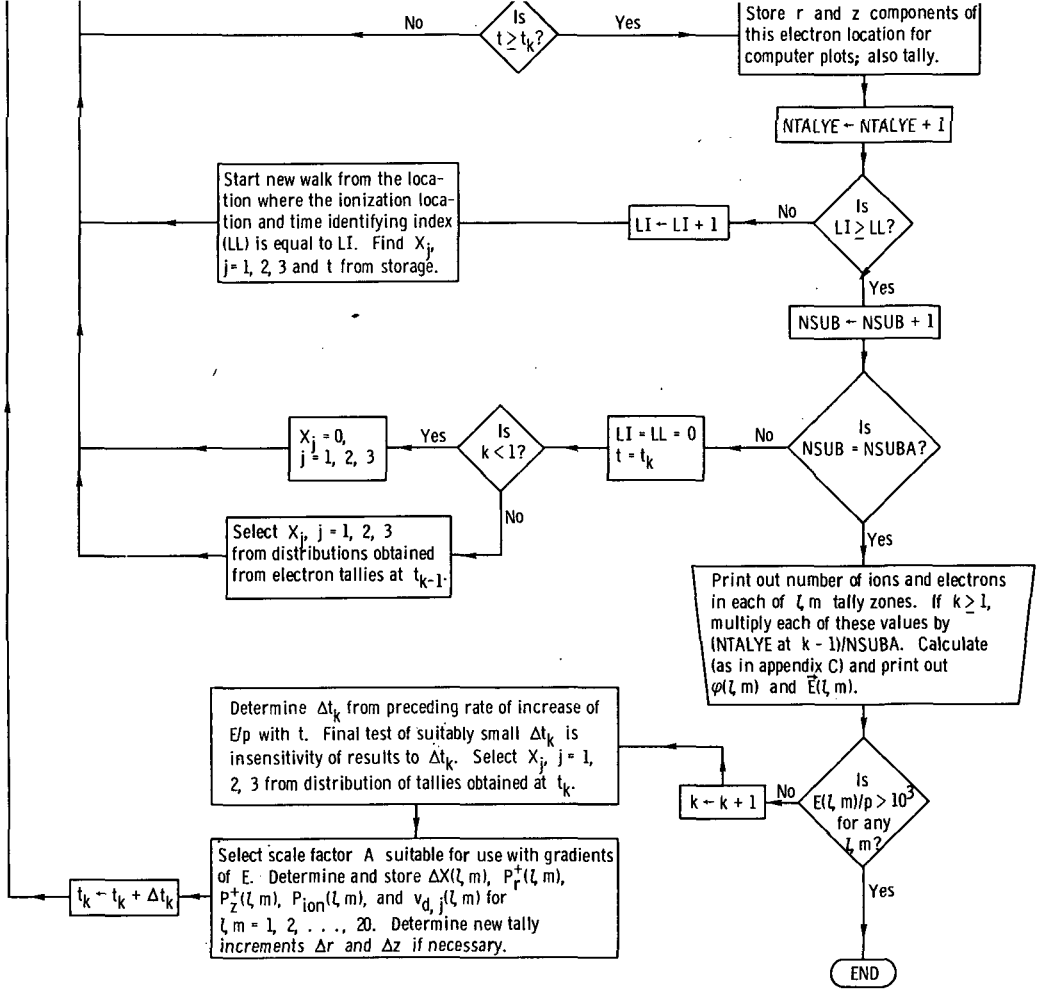

Figure 6. - Flow diagram of main features of computing program for the macroscopic RW.

the step along the j^{th} coordinate is considered positive. Here, for convenience, P_j^+ can be written as

$$P_j^+ = \frac{1}{2} + v_{d,j}\sqrt{\frac{\tau}{8D}} \tag{10}$$

by combining equations (2) and (6). The fourth random number is compared with P_{ion}; and, if it is less than P_{ion}, an ionization event is assumed to occur.

Only the electrons have appreciable diffusive motion or cause ionization, and are, therefore, random walked. It is sufficient to include merely the drift motion of the ions in the calculations.

At various times, t_k, along a macroscopic time scale, the locations of the electrons and ions are recorded for plotting (as in fig. 1) and also tallied (similar to that in ref. 6) to determine their distributions in space. From the tallies, the internal electric field can be determined (see appendix C) and then the probabilities and step sizes from information as on figure 5. These quantities are determined over the physical space of immediate interest and stored in matrix form for convenient access during the walks performed in the next period $t_{k+1} - t_k$. The appropriate (j^{th}) component of the total (external plus induced internal) electric field vector is used in the determination of the vector components P_j and ΔX_j, whereas the magnitude of the total electric field vector is used in the selection of the scalar P_{ion}.

In the early formation period of the avalanche ($N_e \lesssim 10^6$) the internal electric field is negligible and the electron transport coefficients, thus probabilities and step sizes, are constants. As the formation proceeds, the permissable lengths of the time periods Δt_k become less in order to obtain a self-consistent description of collective interaction of charged particles with the field. As the magnitude of the internal electric field reaches and goes beyond that of the external field, the Δt_k must be kept very small (of the order of 10 τ).

The RW can be further facilitated by scaling step size, probabilities, and τ such that equation (9) is generated with a smaller number of (larger) steps as shown in appendix D. Computing time can now be reduced to about 10^{-3} of that needed for the detailed microscopic RW; nevertheless it still becomes excessive for avalanche formation containing more than 10^7 electrons. With such a large number of electrons in the swarm, however, it is not necessary to walk each one. At the higher t_k samplings of about 3×10^3 "test" electrons were found sufficient to represent avalanche growth. Each of such test electrons used to continue the calculations from t_k generates a subavalanche over the period $t_{k+1} - t_k$. The resulting distributions are weighted for the actual number of ions and electrons being represented. In this manner the RW process can be

continued through the final formation periods with total computer time expenditure of the order of 10^2 minutes.

Several possibilities exist for selecting the location of the test electron at the start of each subavalanche. For example, the walks of a fixed number of electrons could be walked from each tally zone at $t = t_k$ and the resulting tallies at t_{k+1} weighted according to the spacial distribution at t_k. As an alternative, a certain fixed fraction of the electrons at t_k could be continued from their respective locations (tally zones). In the present investigation the starting locations were randomly selected from their spatial distributions at t_k. In these later two cases the weighting factor is a constant for any $t_{k+1} - t_k$ time interval. The procedure for random selection of values from an arbitrary distribution when a uniformly distributed set of random numbers is provided by the computer is discussed, for example, in reference 8.

To facilitate calculations and to reduce computer storage requirements, it was assumed that the internal electric field of the avalanche is axisymmetric, thus cylindrical coordinates (r, θ, z) were used for storage (appendix C). In the tallies for the distributions of electrons and ions each element of a matrix represents the number of electrons or ions within an annular zone covering distances $\pm\Delta r/2$ and $\pm\Delta z/2$ about a point (r, z).

A flow diagram which gives a word description of the main features of the computing procedure is given in figure 6.

RESULTS OF THE MACROSCOPIC RANDOM WALK

Only one avalanche will be presented for the RW-on-a-grid type calculation where long formation times, extended to the streamer stage is of interest. This avalanche, based on transport coefficients, has an initial growth equal to that obtained by an averaging of 10^3 formations calculated by means of the microscopic RW method. During the remaining formation time, where many electrons are in the statistical sample, the macroscopic RW continues to generate the structure close to that of an average avalanche.

A plot of the ion locations in such a fully developed avalanche, at an external E/p of 22.5 V-m/N is presented in the first part of figure 7. Here the avalanche profile is obtained by plotting z against radial distance r, instead of x as in figure 1. This gives a better definition of the avalanche profile as it makes more points visible in the outer boundary region due to the scale factor r in the following equation:

$$n(r, z) = \int_0^{2\pi} n(r, \theta, z) r \, d\theta \tag{11}$$

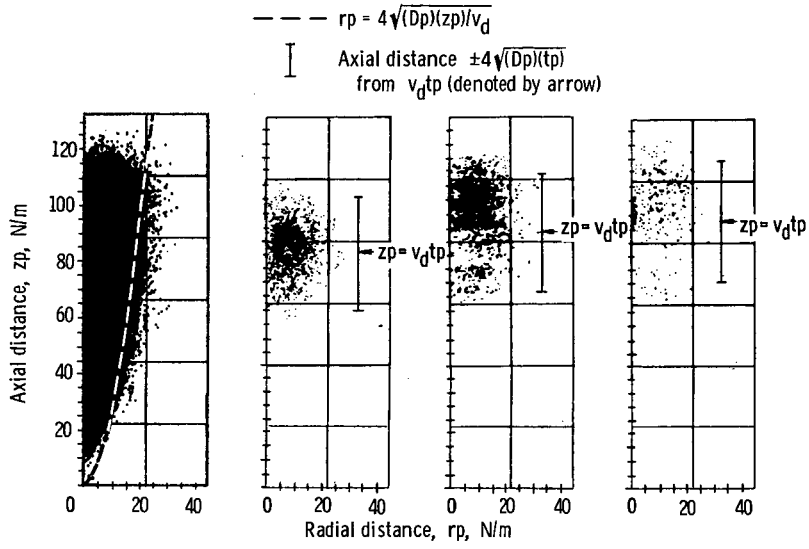

(a) Fully developed ion formation at time parameter $tp = 3.91 \times 10^{-4}$ sec-N/m^2.

(b) Electron swarm at time parameter $tp = 3.4 \times 10^{-4}$ sec-N/m^2; number of subavalanches plotted $N_{sub} = 2788$.

(c) Electron swarm at time parameter $tp = 3.68 \times 10^{-4}$ sec-N/m^2; number of subavalanches plotted $N_{sub} = 7827$.

(d) Electron swarm at time parameter $tp = 3.87 \times 10^{-4}$ sec-N/m^2; number of subavalanches plotted $N_{sub} = 4513$.

Figure 7. - Particle locations obtained by macroscopic RW procedure. Shown first is a fully developed ion formation; next are shown electron swarms at three values of time parameter. External electric field parameter E/p = 22.5 V-m/N.

Twice the diffusion radius, $2r_D \equiv 4\sqrt{Dz/v_d}$, shown by the dashed line fairly well defines the avalanche boundary. It defines the boundary within which $1 - 1/e^4$ (or 98 percent) of the electrons are located. This can be easily obtained by use of equation (B4) of appendix B.

The corresponding electron swarm is shown at three time periods. It is nearly spherical at the first time period since the internal electric field is then quite small. It has a radius close to $2r_D$ and its center is close to the axial location $z = v_d t$. By the end of the second time interval the internal field reaches values close to half that of the external field and now definitely influences the electron pattern. Local minimum and maximum values of internal E occur at zp values of approximately 77 and 100 N-m, respectively. The concentration of electrons is strongly correlated to such field points since α_T, and thus the formation of new electrons and ions, is exponentially dependent on field strength.

As the avalanche buildup continues to tp slightly greater than 3.6×10^{-4} sec-N/m^2, the electric field strength near the axis and in the vicinity of $zp = v_d tp$ increases to magnitudes beyond the external field strength. The last plot on figure 7 shows that there is a corresponding large concentration of electrons (and, therefore, ions) at this location. In

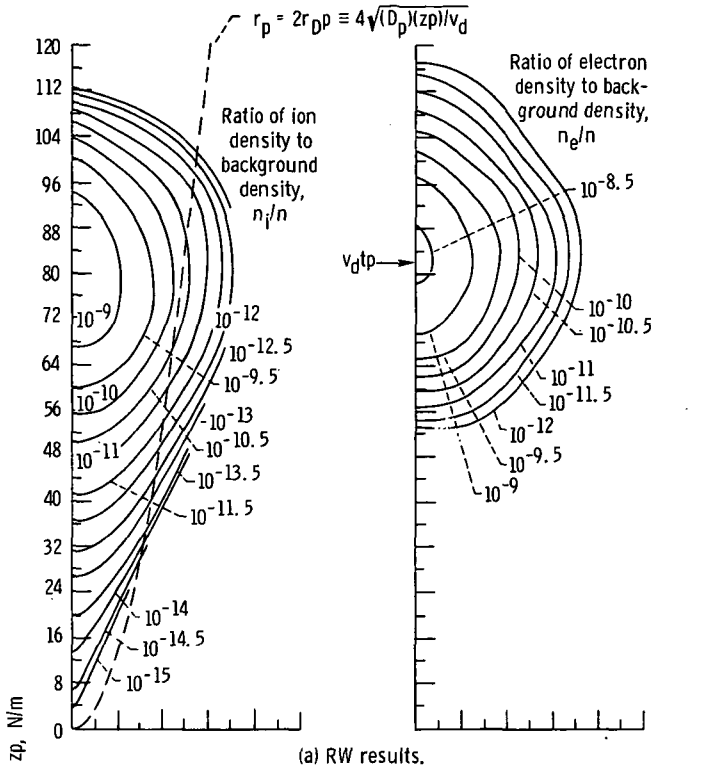

(a) RW results.

(b) Results of constant coefficient theory.

Figure 8. - Contour plots of ion and electron densities divided by background density of helium at formation time $tp = 3.25 \times 10^{-4}$ sec-N/m^2.

fact, the density is so high at $tp = 3.9 \times 10^{-4}$ sec-N/m^2 that only a small sample of electrons can be plotted without a glare in this zone occurring on the plotting screen and obscuring details.

Contour plots of the ion and electron densities are shown in figure 8 at a formation time of 3.25×10^{-4} sec-N/m^2. The RW results (fig. 8(a)) compare quite well with constant coefficient theory (fig. 8(b)) at this tp where the induced electric field is much less than the external field. The diffusion radius profile ($2r_D$) is also shown on the RW ion plot. The exponential falloff of ion, as well as electric, density from the peak regions near $z = v_d t$ and $r = 0$ is apparent.

Marginal distributions, in which integration is over all of the dimensions except the one being studied, are used to present the effects of the internal electric field on density distribution. These often allow a space saving in plotting while preserving the essential features of main interest. Such plots are shown in figures 9 and 10 for both charge species at various formation times. The marginal density distributions ($n_{j,r}$ and $n_{j,z}$) for

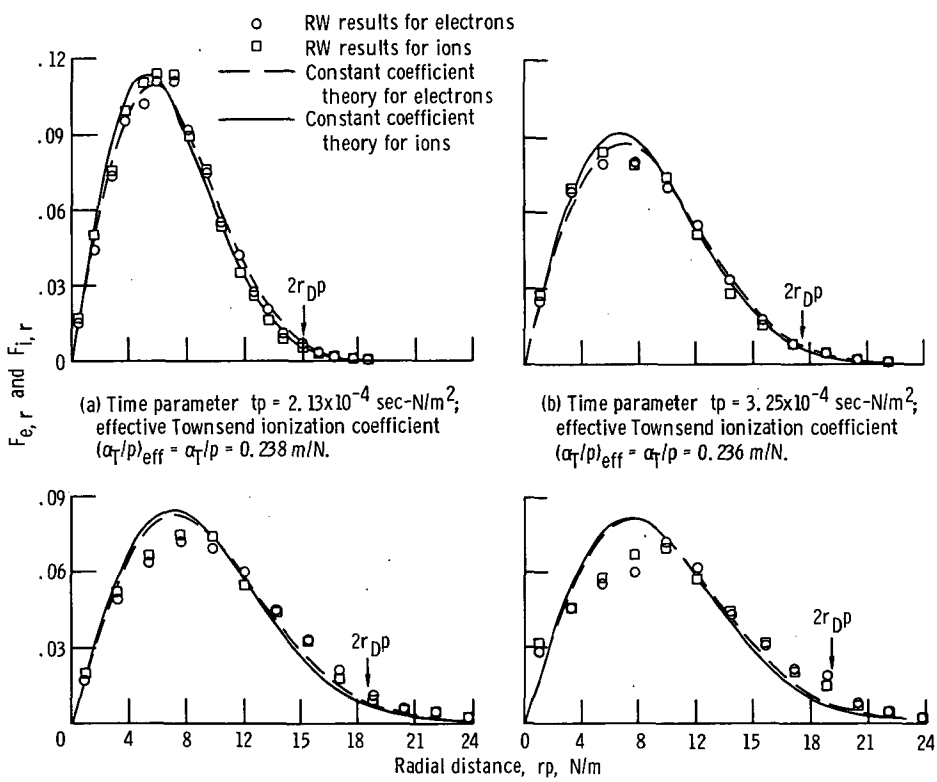

(a) Time parameter $tp = 2.13 \times 10^{-4}$ sec-N/m^2; effective Townsend ionization coefficient $(\alpha_T/p)_{eff} = \alpha_T/p = 0.238$ m/N.

(b) Time parameter $tp = 3.25 \times 10^{-4}$ sec-N/m^2; effective Townsend ionization coefficient $(\alpha_T/p)_{eff} = \alpha_T/p = 0.236$ m/N.

(c) Time parameter $tp = 3.68 \times 10^{-4}$ sec-N/m^2; effective Townsend ionization coefficient $(\alpha_T/p)_{eff} = \alpha_T/p = 0.234$ m/N.

(d) Time parameter $tp = 3.89 \times 10^{-4}$ sec-N/m^2; effective Townsend ionization coefficient $(\alpha_T/p)_{eff} = \alpha_T/p = 0.229$ m/N.

Figure 9. - Marginal density distribution in radial direction at various values of time parameter.

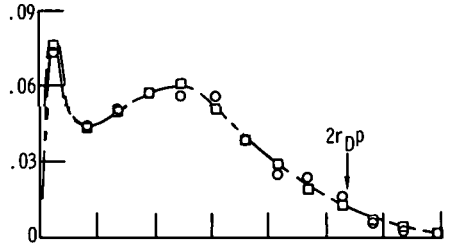

(e) Time parameter $tp = 3.907 \times 10^{-4}$ sec-N/m^2.

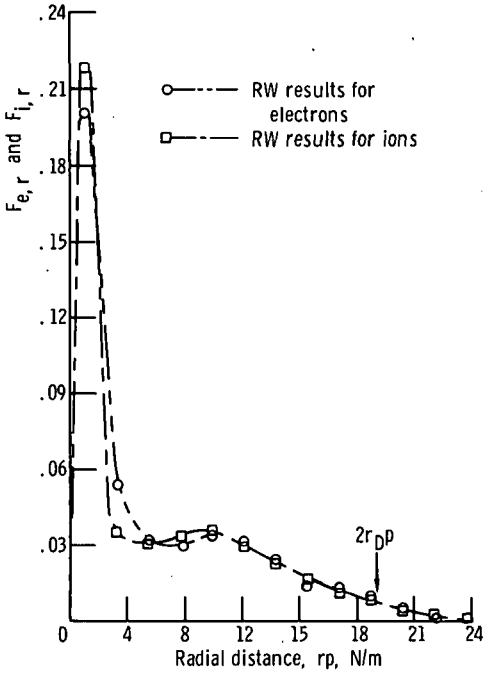

(f) Time parameter $tp = 3.908 \times 10^{-4}$ sec-N/m^2.

Figure 9. - Concluded.

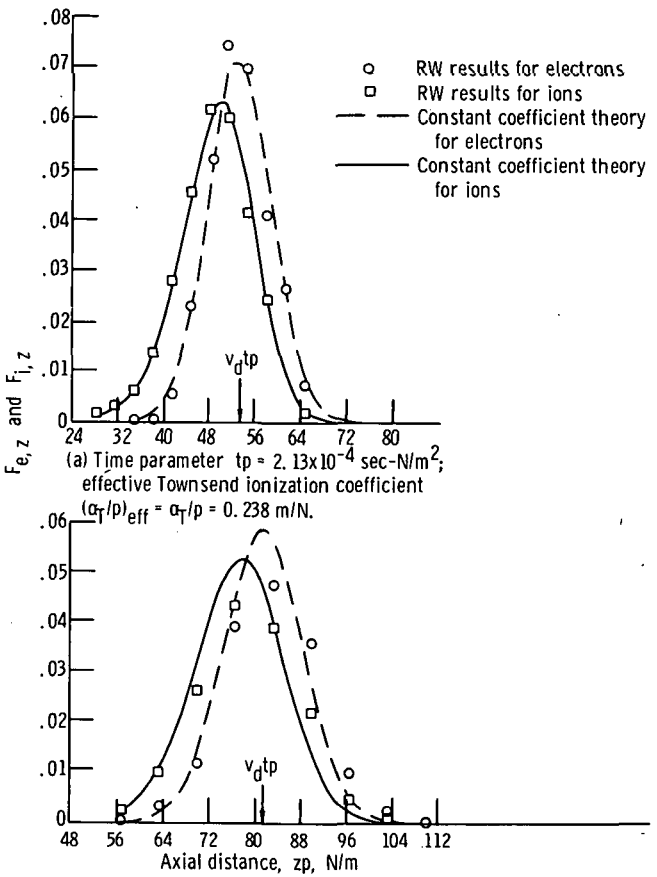

(a) Time parameter $tp = 2.13 \times 10^{-4}$ sec-N/m^2; effective Townsend ionization coefficient $(\alpha_T/p)_{eff} = \alpha_T/p = 0.238$ m/N.

(b) Time parameter $tp = 3.25 \times 10^{-4}$ sec-N/m^2; effective Townsend ionization coefficient $(\alpha_T/p)_{eff} = \alpha_T/p = 0.236$ m/N.

Figure 10. - Marginal density distribution in axial direction at various values of time parameter.

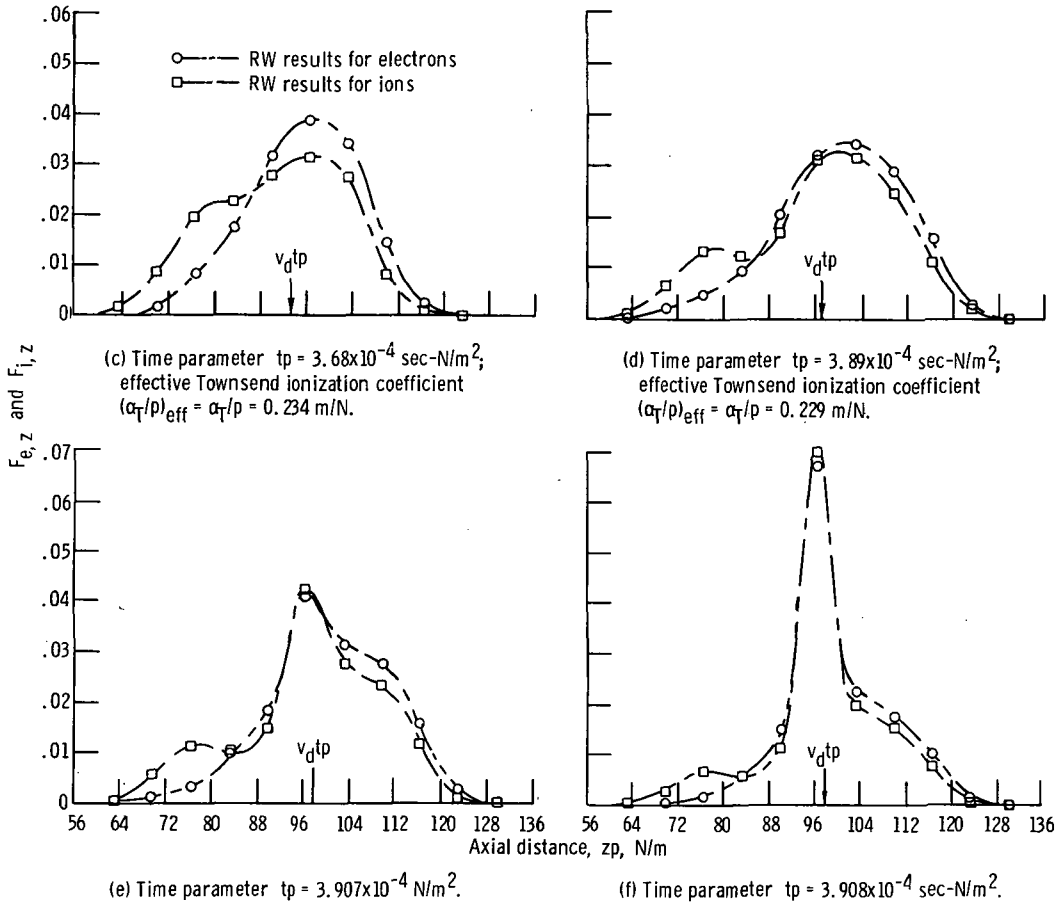

(c) Time parameter $t_p = 3.68 \times 10^{-4}$ sec-N/m^2; effective Townsend ionization coefficient $(\alpha_T/p)_{eff} = \alpha_T/p = 0.234$ m/N.

(d) Time parameter $t_p = 3.89 \times 10^{-4}$ sec-N/m^2; effective Townsend ionization coefficient $(\alpha_T/p)_{eff} = \alpha_T/p = 0.229$ m/N.

(e) Time parameter $t_p = 3.907 \times 10^{-4}$ N/m^2.

(f) Time parameter $t_p = 3.908 \times 10^{-4}$ sec-N/m^2.

Figure 10. - Concluded.

the j^{th} charge species in the r and z directions, respectively, are normalized by dividing by $\exp(\alpha_T v_d t)$ yielding

$$F_{j,r} = n_{j,r} \exp(-\alpha_T v_d t) \equiv \exp(-\alpha_T v_d t) \int_0^\infty \int_0^{2\pi} n_j(r, \theta, z) r \, d\theta \, dz \tag{12}$$

and

$$F_{j,z} = n_{j,z} \exp(-\alpha_T v_d t) \equiv \exp(-\alpha_T v_d t) \int_0^\infty \int_0^{2\pi} n_j(r, \theta, z) r \, d\theta \, dr \tag{13}$$

Keeping the scale factor r with the integration over θ in equation (12) makes the plots of $F_{j,r}$ against r more manageable as it reduces the otherwise exceptionally high values near $r = 0$. Theoretical values of $n_{j,r}$ and $n_{j,z}$ are given in equations (B7) to (B10).

When the internal electric field is negligible, so that the transport coefficients are constant, theory agrees well with the RW results, as expected. The ion distribution

peaks at a very slightly lower radius than the electrons (fig. 9). A difference between the distribution of the two charge species is more noticeable in the axial direction due to the electron drift velocity.

At about a formation time of 3.2×10^{-4} sec-N/m^2 the difference between the RW and the approximate theory becomes noticeable; especially, for the z component of the distributions (fig. 10(b)). The theory is shown only for the r component for the next two time periods selected for plotting; beyond which it is inapplicable. The lines on the subsequent plots are merely fairings through the RW data.

Near tp of 3.6×10^{-4} sec-N/m^2 the z distribution curve starts to neck down at a z location somewhat less than $v_d t$, and bulges out on either side of this z. This is evident in figure 10(c). Note that the computer plots of figure 7 show a tendency for the electron swarm to separate into two zones. The corresponding radial distribution (see fig. 9(d)) now shows an increased concentration of both charge species near the axes as well as a spreading of the outer parts of the curve to radial distances beyond the theoretical curve. As time continues, these trends become more pronounced with a sharp peak forming near the axis and near $v_d t$ in the radial and axial distributions, respectively. This zone is apparent in the last computer plot of figure 7. By this time the induced electric field has exceeded the magnitude of the external field in this region.

Contour plots of the induced electrostatic potential φ are shown in figure 11. The lines of constant φ form sets of approximately circular contours about a region of maximum φ located at a z less than $v_d t$ and a region of minimum φ at a z greater than $v_d t$. The $\varphi = 0$ line is located near a z equal to $v_d t$ during the early formation period.

The internal electric field in the avalanche head is generally predicted to be directed inward toward the center (pp. 78 and 79 of ref. 1) forcing the electrons outward; whereas the internal field in the trailing zone, being rich in ions, is predicted to be outward tending to force the electrons inward. This general pattern is observed in the present study only during the early formation period where the extrema of the field strength are both located on the avalanche axis.

Comparison of figures 11(a) and (b) show again that the constant coefficient theory (eqs. (B12) and (B13)) agrees quite well with RW results at low tp where internal fields are much less than the external value. The contours obtained by both methods look quite alike over much of the field; however, it is the local extrema regions which are decisive in the latter avalanche behavior. A plot of the values of φ extrema against time is shown in figure 12.

As formation time continues beyond 3.6×10^{-4} sec-N/m^2, the region of minimum φ moves to slightly higher radii at times (fig. 11(c) and (d)). Comparison with figure 6 shows that the two extrema regions and the distance between them is essentially the space covered by the electron swarm.

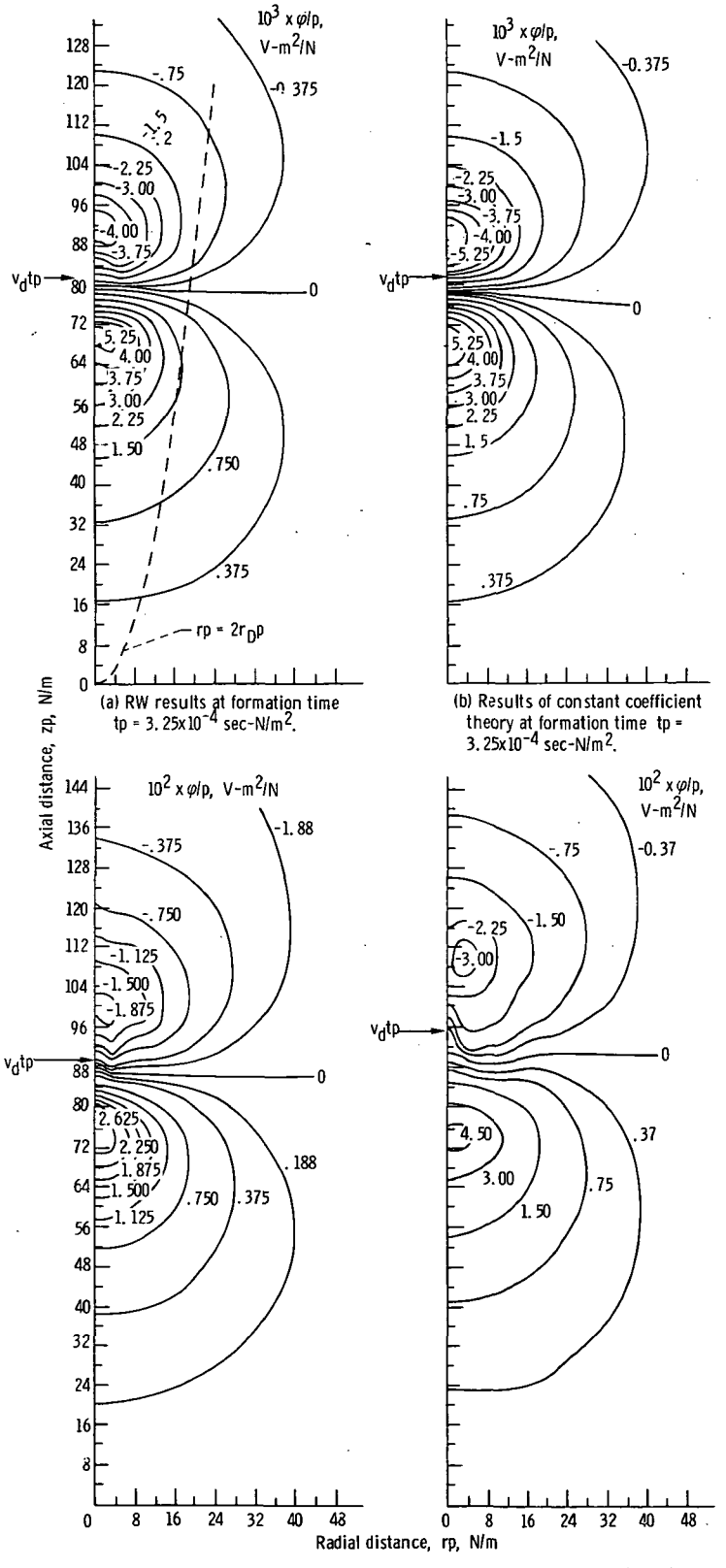

(a) RW results at formation time $t_p = 3.25 \times 10^{-4}$ sec-N/m^2.

(b) Results of constant coefficient theory at formation time $t_p = 3.25 \times 10^{-4}$ sec-N/m^2.

(c) RW results at formation time $t_p = 3.59 \times 10^{-4}$ sec-N/m^2.

(d) RW results at formation time $t_p = 3.80 \times 10^{-4}$ sec-N/m^2.

Figure 11. - Contour plots of induced electrostatic potential φ/p.

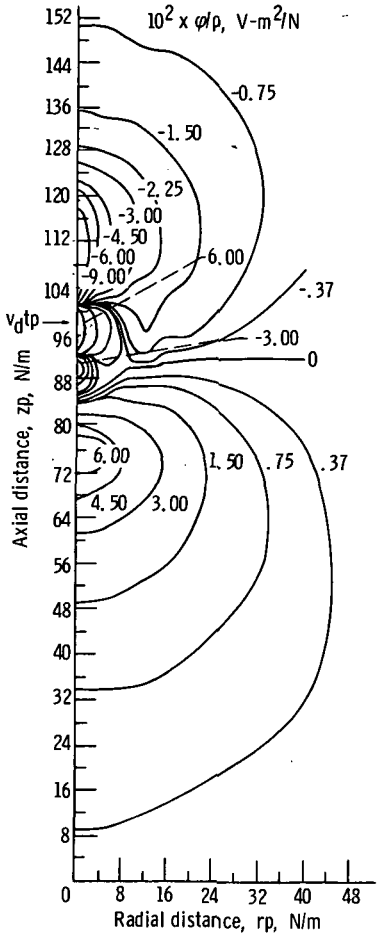

(e) RW results at formation time tp = 3.907×10^{-4} sec-N/m^2.

Figure 11. - Concluded.

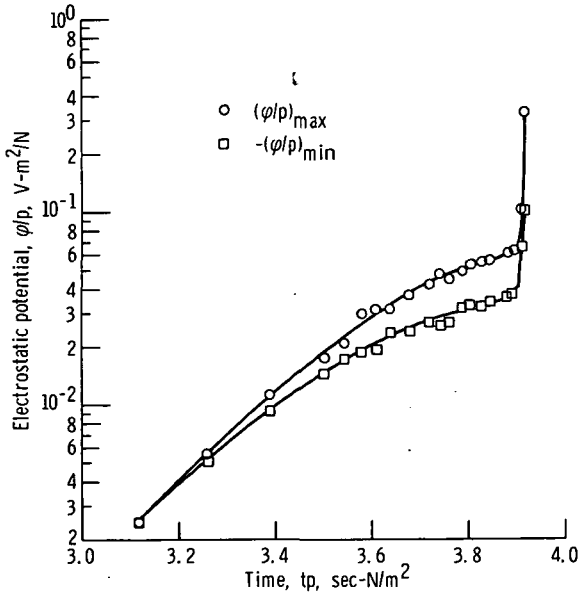

Figure 12. - Buildup of maximum and minimum induced potentials with time.

The contour lines about and in the near vicinity of the regions of extrema often have two or more inflection points oriented such that they indicate enhanced gradients of φ in the radial direction. During the latter stages of avalanche formation, the radial electric field component is found to grow more rapidly than the axial component. A plot of E_r/p against axial distance in the regions of extrema is shown in figure 13 at two radial locations near the axis and at various formation times.

At low tp the radial electric field has approximately a sinusoidal variation as zp increases over the span of the electron swarm. The variation of E_r with z at the inner radial location of figure 13 is more erratic, and indicates a tendency of local charge buildup and relaxation at z values between the two initial extrema (see also fig. 11(e)). This may be an indication of instability caused by the exponential dependence of α_T/p on E/p. This causes a greatly increased rate of electron and ion formation at high E/p locations. The restoring, or stabilizing influence is primarily the drift of electrons in re-

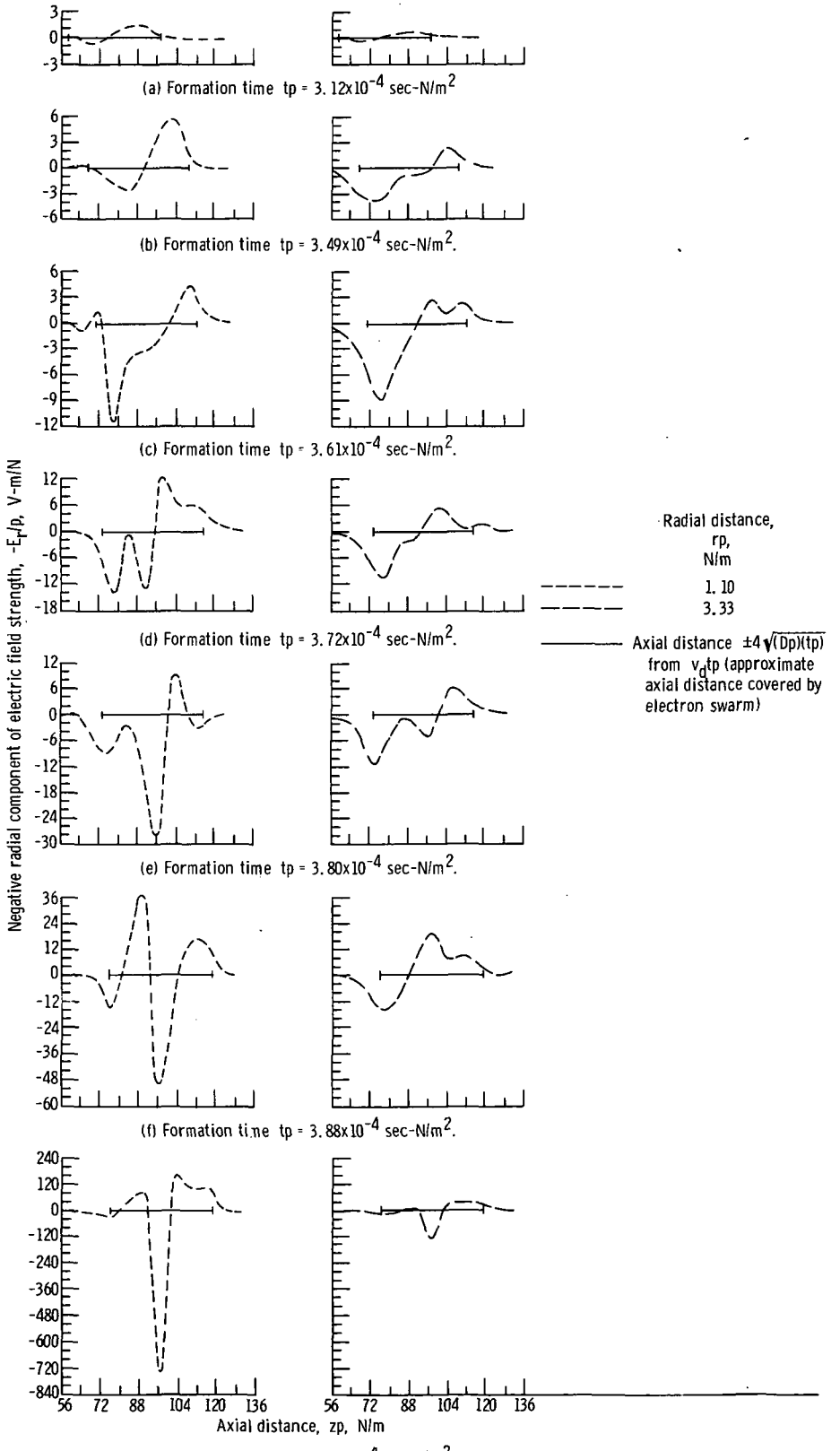

Figure 13. - Buildup of radial components of internal electric field extrema.

sponse to the local electric field. At a formation time of 3.91×10^{-4} sec-N/m^2 the field at the inner radius increases so abruptly that the assumption of axial symmetry can no longer be justified and the calculations were terminated. This abrupt change occurs at a formation of about e^{23} ions which somewhat surpasses the estimate of e^{20} for breakdown in reference 1 (p. 131).

Another indicator of the influence of the induced internal electric field is the effective Townsend ionization coefficient, defined here as

$$\left(\frac{\alpha_T}{p}\right)_{eff} = \left(v_d tp\right)^{-1} \ln\left(\frac{N}{N_o}\right)$$

A retardation of avalanche growth below that calculated with a constant α_T/p equal to $(\alpha_T/p)_{t=0}$ is predicted in references 9 and 10. Such an effect is observed in the present results, as shown in figure 14(a), over about the latter one-third of the formation time.

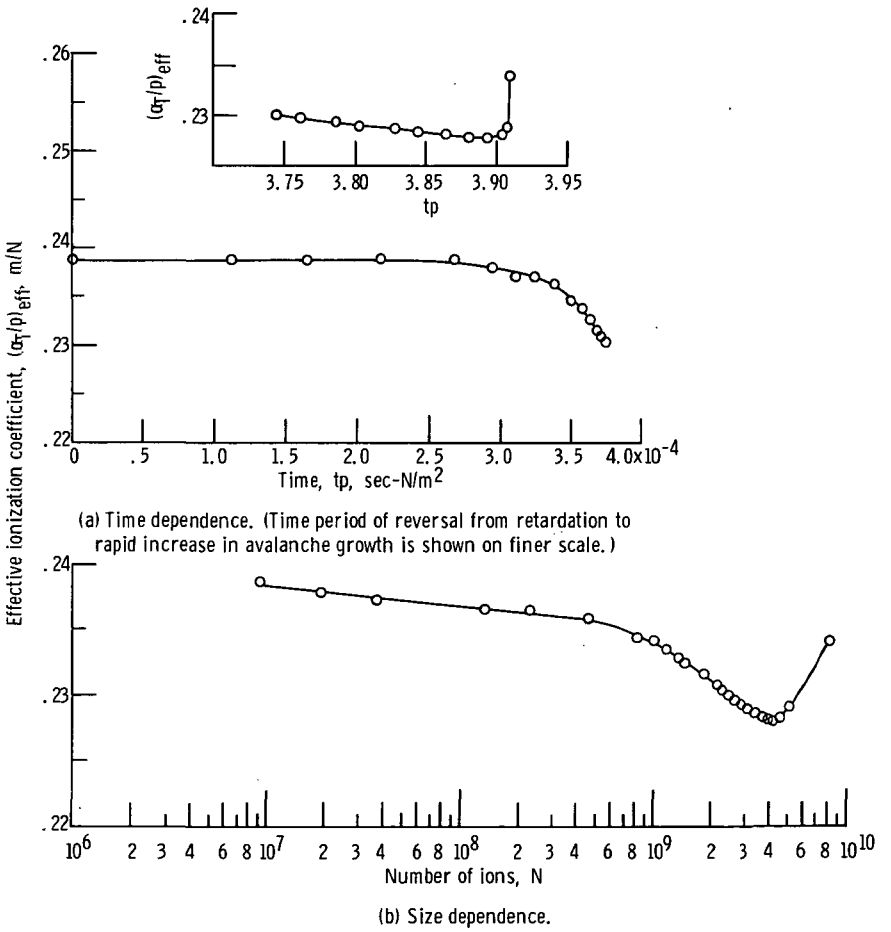

(a) Time dependence. (Time period of reversal from retardation to rapid increase in avalanche growth is shown on finer scale.)

(b) Size dependence.

Figure 14. - Influence of induced internal electric field on effective Townsend ionization coefficient.

This is due primarily to the ions lagging behind the electrons and causing an internal electric field which opposes the external field. At a tp slightly beyond 3.87×10^{-4} sec-N/m^2 however, the high field strengths discussed previously cause local increases in α_T/p which more than offset the retardation process and $(\alpha_T/p)_{eff}$ sharply increases. A plot of $(\alpha_T/p)_{eff}$ against N is given in figure 14(b). The general trends are quite consistent with the experimentally obtained results of reference 11 for N_2.

Use of the $(\alpha_T/p)_{eff}$ of figure 14 in place of $(\alpha_T/p)_{t=0}$ in equations (B8) and (B10) gave little change in the theoretical ion marginal distributions of figures 9 and 10. Use of $(\alpha_T/p)_{eff}$ in the electrostatic potential calculation of equations (B11) and (B12), however, noticeably improved agreement between approximate theory and the RW results in the intermediate time periods.

The assumption that step size has only a weak spatial dependence, used in the derivation of equation (7) can now be further appraised. The ratio of step size ΔX_j to the step size at z = 0 is plotted in figure 15 against zp at a low value of rp and a high value of tp where the internal field, and thus transport coefficients, undergo extreme variations. This is compared to the dependence of other quantities entering the macroscopic RW calculations: the z component of bias, $P_z^+ - P_z^-$, and the probability of ionization P_{ion}. Step size is shown to be quite insensitive to distance, especially compared to the large changes experienced in the other two RW quantities.

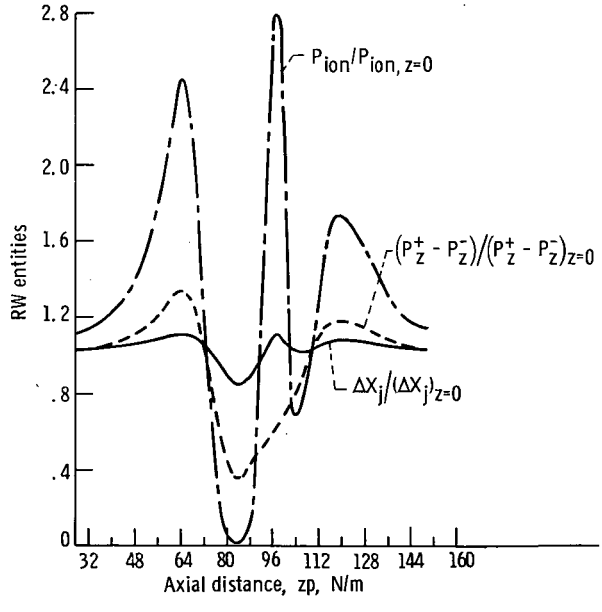

Figure 15. - Spatial variation of step size ΔX_j, z component of bias $P_z^+ - P_z^-$, and probability of ionization P_{ion}. Radial distance from avalanche axis rp = 1.1 N/m; formation time tp = 3.8 sec-N/m^2; external electric field strength E/p = 22.5 V-m/N.

CONCLUSIONS

The present random walk (RW) study of avalanche formation in helium leads to the following conclusions:

1. The results of random walks utilizing simulation of the electron trajectories in an avalanche in minute detail show that the electron transport coefficients very quickly relax to local equilibrium values. This enables the use of an alternate RW-on-a-grid concept in which the step sizes and probabilities are based on equilibrium transport coefficients. Thus they are functions only of the local electric field and background density of neutrals. The concomitant reduction in computer time expenditure makes calculations of large avalanche formations feasible. By only a simple repetitious procedure a self-consistent internal electric field solution is obtained. Collective long range Coulomb interactions as well as short range elastic and inelastic collisions are accounted for.

2. Results obtained by this method at an E/p of 22.5 V-m/N show that the internal electrostatic potential φ pattern in its early stage of formation has minumum and maximum values of potential on the avalanche axis. The axial distance over which large φ gradients appear is essentially that spanned by the electron swarm. As avalanche growth continues, the minimum φ region moves to slightly higher radii. Within the separation distance between the two extrema, several other large φ-gradient zones form and die out in a manner which appears to be random in time. At a generalized formation time tp slightly greater than 3.87×10^{-4} sec-N/m, the internal electric field abruptly increases far beyond the magnitude of the external field.

3. The tail region behind the electron swarm, has a positive charge which opposes the external field. This tends to reduce the effective ionization coefficient, which is an indicator of the avalanche growth. At the time of the abrupt increase of the magnitudes of the internal field strength, the electron and ion formation rate in the region of the φ extrema increases to the extent that it offsets the growth retardation influence in the tail region. The effective ionization coefficient then sharply increases.

4. Theory, based on constant transport coefficients, gives good results only in the early formation periods of the avalanche where internal electric fields are much less than the external fields. Here, electron and ion density distributions, as well as the general contours of the internal electrostatic potential are quite satisfactory. Some noticeable improvement in the theoretical φ contours is obtained by replacing Townsend's first ionization coefficient based on the external field by the effective ionization coefficient for the formation time of interest.

Lewis Research Center,
National Aeronautics and Space Administration,
Cleveland, Ohio, January 4, 1973,
503-10.

APPENDIX A

SYMBOLS

A	scale factor
a	combination of variables defined by eq. (C7)
b	combination of variables defined by eq. (C8)
D	coefficient of diffusion
E	electric field strength
$\mathscr{E}$	elliptic integral of second kind
e	electrostatic unit of charge
$F_{j,r}$	normalized marginal density distribution in radial direction
$F_{j,z}$	normalized marginal density distribution in axial direction
$\mathscr{F}$	elliptic integral of first kind
$\mathscr{K}$	complete elliptic integral of first kind
N	number
n	particle density (with no subscripts this refers to neutral background particles)
$n_{j,r}$	marginal density distribution of j^{th} species in radial direction
$n_{j,z}$	marginal density distribution of j^{th} species in axial direction
P_{ion}	probability that encounter between electron and neutral atom causes ionization
P_j^+	probability that j^{th} component of step will be in positive direction
P_j^-	probability that j^{th} component of step will be in negative direction
p	pressure
Q_a	total absorption cross section of electrons colliding with background neutral atoms
R	radial distance in spherical coordinates
r	radial distance, in cylindrical coordinates, from axis of avalanche
r_D	diffusion radius
S	source density
t	time
v	velocity

$\bar{v}$ mean velocity obtained by integrating over distribution of total velocity

W probability density

X_j distance in j^{th} direction used in macroscopic descriptions

x_j distance in j^{th} direction used in microscopic descriptions

x, y, z Cartesian avalanche coordinates; x and y are in a plane perpendicular to z; z is axial distance along avalanche axis

α_T Townsend first ionization coefficient

Γ combination of variables defined by eq. (C9)

γ combination of variables defined by eq. (C13)

δ small finite increment

ϵ_o capacitivity of vacuum

$\bar{\epsilon}_r$ mean electron energy obtained by integrating over distribution of random energies

η dimensionless distance in avalanche space

Θ angle between field and source vectors in cylindrical coordinates

θ angle

ξ radius ratio

ρ charge density

τ mean free time

φ induced electrostatic potential

ψ supplement of angle Θ

Subscripts:

a absorption

D diffusion

d drift

e electron

i ion

ion ionization event

o initial

r radial

z axial

APPENDIX B

DERIVATION OF MACROSCOPIC DESCRIPTIVE EQUATIONS

For the range of electric field strength of interest here, a diffusion coefficient for an isotropic medium can be used (see table I of ref. 2). The flux of electrons about a mean (drift) velocity $\vec{v}_d$ due to diffusion is then given by Fick's law as (ref. 12)

$$n_e(\vec{\vec{v}} - \vec{v}_d) = -D \nabla n_e$$

Substituting this into the continuity equation,

$$\frac{\partial n_e}{\partial t} + \nabla \cdot n_e \vec{\vec{v}} = S(\vec{r})$$

where $S(\vec{r}) = \alpha_T v_d n_e$ accounts for sources, gives the electron transport equation

$$\frac{\partial n_e}{\partial t} = - \nabla \cdot n_e \vec{v}_d + \nabla \cdot (D \nabla n_e) + \alpha_T v_d n_e \tag{B1}$$

Here α_T is the Townsend first ionization coefficient and $\alpha_T v_d n_e$ is the increase of the number of electrons per unit time per unit volume due to ionization events. Only singly charged ions are considered.

The ions are cold and have a negligible random velocity. Their transport equation is simply

$$\frac{\partial n_i}{\partial t} = - \nabla \cdot n_i \vec{v}_{d,i} + \alpha_T v_d n_e \tag{B2}$$

Equations (B1) and (B2) are coupled through Poisson's equation,

$$\nabla^2 \varphi = \frac{-e(n_i - n_e)}{\epsilon_o} \tag{B3}$$

and the dependence of the transport coefficients on the electric field vector which is equal to $-\nabla\varphi$ plus the external electric field.

Density Distributions

For constant coefficients equations (B1) and (B2) can be solved immediately. The electron density is

$$n_e = \frac{1}{(4\pi Dt)^{3/2}} \exp\left[\alpha_T v_d t - \frac{r^2 + (z - v_d t)^2}{4Dt}\right] \tag{B4}$$

in cylindrical coordinates with azimuthal symmetry. Here the avalanche is assumed to start from one electron. The ion density can then be obtained from

$$n_i = \alpha_T v_d \int_0^t n_e \, dt' \tag{B5}$$

if it assumed that the ion drift is negligible. Using equation (B4) in equation (B5) gives

$$n_i = \alpha_T v_d \int_0^t \frac{1}{(4\pi Dt')^{3/2}} \exp\left[\alpha_T v_d t' - \frac{r^2 + (z - v_d t')^2}{4Dt'}\right] dt' \tag{B6}$$

Equations (B4) and (B6) are used in the avalanche studies of references 9 and 13.

Marginal distributions are often used to reduce the number of variables required for plotting results. Integrating densities, n_e and n_i, over r and θ gives the marginal distributions, $n_{e,z}$ and $n_{i,z}$, in z as follows. By definition

$$n_{e,z} = \int_0^\infty \int_0^{2\pi} n_e r \, d\theta \, dr$$

Substituting equation (B4) for n_e yields

$$n_{e,z} = \frac{2\pi}{(4\pi Dt)^{3/2}} \exp\left[\alpha_T v_d t - \frac{(z - v_d t)^2}{4Dt}\right] \int_0^\infty r \exp\left(-\frac{r^2}{4Dt}\right) dr$$

$$= \frac{1}{\sqrt{4\pi Dt}} \exp\left[\alpha_T v_d t - \frac{(z - v_d t)^2}{4Dt}\right] \tag{B7}$$

Using this result in equation (B5) yields the following expression for ions:

$$n_{i,z} = \frac{\alpha_T v_d}{\sqrt{\pi}} \int_0^t \frac{1}{\sqrt{4Dt'}} \exp\left[\alpha_T v_d t' - \frac{(z - v_d t')^2}{4Dt'}\right] dt' \tag{B8}$$

In like manner

$$n_{e,r} = \int_0^\infty \int_0^{2\pi} n_e r \, d\theta \, dz$$

$$= \frac{2\pi \sqrt{4Dt}\, r}{(4\pi Dt)^{3/2}} \exp\left(\alpha_T v_d t - \frac{r^2}{4Dt}\right) \int_{-v_d t/\sqrt{4Dt}}^\infty e^{-\eta^2} \, d\eta$$

where

$$\eta = \frac{(z - v_d t)}{\sqrt{4Dt}}$$

Finally

$$n_{e,r} = \frac{r}{4Dt} \exp\left(\alpha_T v_d t - \frac{r^2}{4Dt}\right)\left[1 + \operatorname{erf}\left(\frac{v_d t}{\sqrt{4Dt}}\right)\right]$$

For formation times of interest $\operatorname{erf}(v_d t/\sqrt{4Dt}) \approx 1$, and

$$n_{e,r} = \frac{r}{2Dt} \exp\left(\alpha_T v_d t - \frac{r^2}{4Dt}\right) \tag{B9}$$

Using this result in equation (B5) gives

$$n_{i,r} = \alpha_T v_d r \int_0^t \frac{1}{2Dt'} \exp\left(\alpha_T v_d t' - \frac{r^2}{4Dt'}\right) dt' \tag{B10}$$

Equations (B7) to (B10) can be normalized by dividing by $\exp(\alpha_T v_d t)$.

Potential Distributions

Use of the assumption of constant transport coefficients in the preceding derivations results in expressions which show that the electrons then diffuse as a spherically symmetric swarm, the center of which is at $z = v_d t$ on the avalanche axis of symmetry. This simplification in turn permits determination of the electrostatic potential φ_e due to the electron distribution in space.

The electrostatic potential for electrons can be obtained from

$$\varphi_e(\vec{r},t) = \frac{1}{4\pi\epsilon_o}\int \frac{\rho_e(\vec{r}',t)}{|\vec{r}-\vec{r}'|}\,d^3r'$$

where integration is over the whole field of the electrons. In like manner the potential for ions is

$$\varphi_i(\vec{r},t) = \frac{1}{4\pi\epsilon_o}\int \frac{\rho_i(\vec{r}',t)}{|\vec{r}-\vec{r}'|}\,d^3r'$$

Using equation (B5) and singly charged particles

$$\rho_i(\vec{r},t) = -\alpha_T v_d \int_0^t \rho_e(\vec{r},t')dt'$$

so that

$$\varphi_i(\vec{r},t) = -\alpha_T v_d \int_0^t \varphi_e(\vec{r},t')dt' \qquad \text{(B11)}$$

The total potential φ is then the sum of φ_e and φ_i.

Let R denote radial distance in the spherical (avalanche space) system. The well-known potential equation for such a charge distribution is

$$\varphi_e(R,t) = \frac{1}{\epsilon_o R}\int_0^R R'^2\rho_e(R',t)dR' + \frac{1}{\epsilon_o}\int_R^\infty R'\rho_e(R',t)dR'$$

Using equation (B4) gives

$$\varphi_e(R,t) = -\frac{e\exp(\alpha_T v_d t)}{\pi^{3/2}\epsilon_o}\left[\frac{1}{R}\int_0^{R/R_D}\xi^2 e^{-\xi^2}\,d\xi + \frac{1}{R_D}\int_{R/R_D}^{\infty}\xi e^{-\xi^2}\,d\xi\right]$$

where $\xi = R/R_D$ and $R_D = \sqrt{4Dt}$. Finally

$$\varphi_e(R,t) = -\frac{e\exp(\alpha_T v_d t)}{4\pi\epsilon_o R}\,\mathrm{erf}\left(\frac{R}{R_D}\right)$$

where the method of integration by parts was used in evaluation of the first integral.[1]

Changing back to cylindrical coordinates in laboratory space gives

$$\varphi_e(r,z,t) = -\frac{e\exp(\alpha_T v_d t)}{4\pi\epsilon_o\sqrt{r^2 + \left(z - v_d t\right)^2}}\,\mathrm{erf}\left[\frac{r^2 + \left(z - v_d t\right)^2}{4Dt}\right]^{1/2} \tag{B12}$$

Substituting equation (B12) into equation (B11) then yields

$$\varphi_i(r,z,t) = \frac{\alpha_T v_d e}{4\pi\epsilon_o}\int_0^t \frac{\exp(\alpha_T v_d t')}{\sqrt{r^2 + \left(z - v_d t'\right)^2}}\,\mathrm{erf}\left[\frac{r^2 + \left(z - v_d t'\right)^2}{4Dt'}\right]^{1/2} dt' \tag{B13}$$

---

[1]The radial electric field E_R is now given by

$$E_R = -\frac{\partial\varphi}{\partial R} = \frac{e\exp(\alpha_T v_d t)}{4\pi\epsilon_o R_D^2}\,\frac{d}{d\,\frac{R}{R_D}}\left[\frac{\mathrm{erf}\left(\frac{R}{R_D}\right)}{\frac{R}{R_D}}\right]$$

which agrees with equation (4) of reference 9.

APPENDIX C

DETERMINATION OF INTERNAL ELECTRIC FIELD FROM TALLIES OF ELECTRONS AND IONS

Axial symmetry is assumed so that the induced electric field has only a radial, E_r, and an axial, E_z, component. The field and source points are located at r, θ, z and r', θ', z', respectively. Using Coulombs law, and MKS units, the induced electrostatic potential for singly charged ions is

$$\varphi(r,z) = \frac{e}{4\pi\epsilon_o} \iiint \frac{n_i(r',z') - n_e(r',z')}{\sqrt{r^2 + r'^2 - 2rr'\cos\Theta + (z-z')^2}} r'\,dr'\,d\Theta\,dz \qquad (C1)$$

where $\Theta = \theta - \theta'$ and the integration is over the whole space occupied by the avalanche. By differentiation it follows that

$$E_r(r,z) = \frac{e}{4\pi\epsilon_o} \iiint \frac{\left[n_i(r',z') - n_e(r',z')\right](r - r'\cos\Theta)}{\left[r^2 + r'^2 - 2rr'\cos\Theta + (z-z')^2\right]^{3/2}} r'\,dr'\,d\Theta\,dz \qquad (C2)$$

and

$$E_z(r,z) = \frac{e}{4\pi\epsilon_o} \iiint \frac{\left[n_i(r',z') - n_e(r',z')\right](z - z')}{\left[r^2 + r'^2 - 2rr'\cos\Theta + (z-z')^2\right]^{3/2}} r'\,dr'\,d\Theta\,dz \qquad (C3)$$

The integrations over Θ can be expressed in terms of elliptic integrals. As long as r' and z' do not equal r and z simultaneously, equations (C1) to (C3) can be reduced, for example, by using equation (5) page 154 and equation (4) page 156 of reference 14. Indicating the contribution of the source points to φ, E_r, and E_z in the neighborhood of the field points by $\delta\varphi$, δE_r, and δE_z and integrating over the remaining source volume gives

$$\varphi = \delta\varphi + \frac{e}{\pi\epsilon_o} \iint \frac{n_i - n_e}{\sqrt{a + b}} \mathcal{K}(\Gamma) r' \, dr' \, dz' \tag{C4}$$

$$E_r = \delta E_r + \frac{e}{\pi\epsilon_o} \iint \frac{n_i - n_e}{b\sqrt{a + b}} \left[\frac{br - ar'}{a - b} \mathcal{E}(\Gamma) + r' \mathcal{K}(\Gamma) \right] r' \, dr' \, dz' \tag{C5}$$

and

$$E_z = \delta E_z + \frac{e}{\pi\epsilon_o} \iint \frac{n_i - n_e}{(a - b)\sqrt{a + b}} (z - z') \mathcal{E}(\Gamma) r' \, dr' \, dz' \tag{C6}$$

where

$$a \equiv r^2 + r'^2 + (z - z')^2 \tag{C7}$$

$$b \equiv 2rr' \tag{C8}$$

and

$$\Gamma \equiv \sqrt{\frac{2b}{a + b}} \tag{C9}$$

The identity

$$\frac{\cos \Theta}{(a - b \cos \Theta)^{3/2}} = - \frac{1}{b\sqrt{a - b \cos \Theta}} + \frac{a}{b} \frac{1}{(a - b \cos \Theta)^{3/2}}$$

was used in simplifying equation (C2).

When r approaches r' and z approaches z', slightly more cumbersome expression result. The distance of closest approach between charged particles is assumed to be $n_e^{-1/3}$. It is now convenient to replace Θ with its supplement, $\psi = \pi - \Theta$. Then, using, for example, equations (4) and (3) of pages 154 and 156, respectively, of reference 14, results in

$$\delta\varphi = \frac{e}{2\pi\epsilon_o} \iint \left[n_i(r', z') - n_e(r', z')\right] \sqrt{\frac{2}{b}}\, \mathcal{F}\left(\gamma, \frac{1}{\Gamma}\right) r'\, dr'\, dz' \tag{C10}$$

$$\delta E_r = \frac{e}{2\pi\epsilon_o} \iint \left[n_i(r', z') - n_e(r', z')\right] \left\{ \sqrt{\frac{2}{b}} \frac{r + r'}{a + b}\, \mathcal{F}\left(\gamma, \frac{1}{\Gamma}\right) + \frac{2(rb - ar')}{(a - b)(a + b)} \left[\sqrt{\frac{2}{b}}\, \mathcal{E}\left(\gamma, \frac{1}{\Gamma}\right) - \frac{\sin \delta\psi}{\sqrt{a - b \cos \delta\psi}} \right] \right\} r'\, dr'\, dz' \tag{C11}$$

$$\delta E_z = \frac{e}{2\pi\epsilon_o} \iint \left[n_i(r', z') - n_e(r', z')\right] \left\{ \frac{z - z'}{a + b} \sqrt{\frac{2}{b}}\, \mathcal{F}\left(\gamma, \frac{1}{\Gamma}\right) + \frac{2b(z - z')}{(a - b)(a + b)} \left[\sqrt{\frac{2}{b}}\, \mathcal{E}\left(\gamma, \frac{1}{\Gamma}\right) - \frac{\sin \delta\psi}{\sqrt{a - b \cos \delta\psi}} \right] \right\} r'\, dr'\, dz' \tag{C12}$$

where

$$\gamma = \arcsin \sqrt{\frac{b(1 + \cos \delta\psi)}{a + b}} \tag{C13}$$

Here the distance of closest approach in the ψ direction is expressed as arc length $r\,\delta\psi$, or

$$\delta\psi = \frac{1}{r n_e^{1/3}} \tag{C14}$$

As r approaches r' and z approaches z', Γ approaches 1 and

$$\gamma \to \sin^{-1} \sqrt{\frac{1 + \cos \delta\psi}{2}}$$

Then

$$\mathscr{E}\left(\gamma, \frac{1}{\Gamma}\right) - \mathscr{E}(\gamma, 1) = \sin\gamma = \sqrt{\frac{1 + \cos\,\delta\psi}{2}}$$

and

$$\mathscr{F}\left(\gamma, \frac{1}{\Gamma}\right) - \mathscr{F}(\gamma, 1) = \ln\,\mathrm{tn}\left(\frac{\gamma}{2} + \frac{\pi}{4}\right)$$

Thus for small separation distance between field and source points

$$\delta\varphi = \frac{e}{2\pi\epsilon_o r} \iint \left[n_i(r', z') - n_e(r', z')\right] \ln\,\mathrm{tn}\left(\frac{\gamma}{2} + \frac{\pi}{4}\right) r'\,dr'\,dz' \qquad \text{(C15)}$$

$$\delta E_r = \frac{e}{4\pi\epsilon_o r^2} \iint \left[n_i(r', z') - n_e(r', z')\right] \ln\,\mathrm{tn}\left(\frac{\gamma}{2} + \frac{\pi}{4}\right) r'\,dr'\,dz' \qquad \text{(C16)}$$

and

$$\delta E_z = \frac{e}{8\pi\epsilon_o r^3} \iint n_e^{-1/3}\left[n_i(r', z') - n_e(r', z')\right] \ln\,\mathrm{tn}\left(\frac{\gamma}{2} + \frac{\pi}{4}\right) r'\,dr'\,dz' \qquad \text{(C17)}$$

In the computing procedure the ion and electron density distribution in r, z space is represented in matrix form. Each element of a density matrix represents the number of ions or electrons inside a thin or small annular source volume (zone) equal to $2\pi r'\,\Delta r'\,\Delta z'$ (fig. 4). The number of particles $N(i,j)$ in each zone is obtained during the random walks by a tally procedure at the t_k time periods of interest. The φ, E_r, and E_z are assumed constant in each of such small field zones. Using this approximation in equations (C4) to (C17) yields

$$\varphi(l, m) = \frac{e}{4\pi^2\epsilon_o}\left\{\left[N_i(l, m) - N_e(l, m)\right] r^{-1} \ln\,\mathrm{tn}\left(\frac{\gamma}{2} + \frac{\pi}{4}\right) + 2 \sum_{j,k=1}^{20}{}' \frac{\left[N_i(j,k) - N_e(j,k)\right]}{\sqrt{a + b}} \mathscr{K}(\Gamma)\right\} \qquad \text{(C18)}$$

$$E_r(l,m) = \frac{e}{8\pi^2\epsilon_o}\left\{\left[N_i(l,m) - N_e(l,m)\right]r^{-2}\ln\tan\left(\frac{\gamma}{2}+\frac{\pi}{4}\right)\right.$$

$$\left. + 4\sum_{j,k=1}^{20}{}' \frac{N_i(j,k) - N_e(j,k)}{b\sqrt{a+b}}\left[\frac{br - ar'}{a-b}\mathscr{E}(\Gamma) + r'\mathscr{K}(\Gamma)\right]\right\} \qquad (C19)$$

and

$$E_z(l,m) = \frac{e}{16\pi^2\epsilon_o}\left\{ N_i(l,m) - N_e(l,m)\right]r^{-3}n_e^{-1/3}\ln\tan\left(\frac{\gamma}{2}+\frac{\pi}{4}\right)$$

$$\left. + 8\sum_{j,k=1}^{20}{}' \frac{N_i(j,k) - N_e(j,k)}{(a-b)\sqrt{a+b}}(z - z')\mathscr{E}(\Gamma)\right\} \qquad (C20)$$

where the prime marks on the summation signs indicate exclusion of $j = l$ and $k = m$ combination. The r, r', z, and z' distances which enter the equation are measured to the midpoints of the annular zone; that is, the inner radii + $\Delta r/2$ and to the lower z boundary + $\Delta z/2$. Limitation of each group of zones to 400 was found to provide sufficiently accurate charge distributions and yet be within the limits of a convenient amount of computer storage.

APPENDIX D

SCALING THE MACROSCOPIC RW

In the early time periods when the avalanche is undergoing relatively slow changes, the calculation procedure can be further facilitated by using a scale factor, A. Let

$$\Delta X_j' = \sqrt{A}\,\Delta X_j$$

$$P_j^{+\prime} - P_j^{-\prime} = \sqrt{A}\left(P_j^{+} - P_j^{-}\right)$$

$$P_{ion}' = AP_{ion}$$

and

$$\tau' = A\tau$$

Then using equations (4) and (6)

$$D_j' = \frac{\left(\Delta X_j'\right)^2}{2\tau'} = D_j$$

and

$$v_{d,j}' = \sqrt{\frac{2D'}{\tau'}}\left(P_j^{+\prime} - P_j^{-\prime}\right) = v_{d,j}$$

From the definition of P_{ion},

$$\alpha_T' = \frac{P_{ion}}{v_d'\tau'} = \alpha_T$$

Thus the coefficients in the electron transport equation remain unchanged but the RW is performed with a fewer number of steps. In helium at an E/p of 22.5 V-m/N the scale factor must not get much greater than 40 in order to keep $P_j^{+\prime}$ and P_{ion}' less than unity.

At higher formation times the use of scale factor is of little value as it must be reduced to nearly one in order to keep τ' and $\Delta X_j'$ much less than the time and spatial increments within which there are sizable avalanche changes.

REFERENCES

1. Raether, Heinz: Electron Avalanches and Breakdown in Gases. Butterworth and Co., 1964.
2. Englert, Gerald W.: Random Walk Theory of Elastic and Inelastic Time Dependent Collisional Processes in an Electric Field. Zeit. f. Naturforsch., vol. 26A, no. 5, May 1971, pp. 836-848.
3. Englert, Gerald W.: Random Walk Study of Electron Motion in Helium in Crossed Electromagnetic Fields. NASA TN D-6648, 1972.
4. Englert, G. W.: Physical Interrelation Between Fokker-Planck and Random Walk Models with Application to Coulomb Interactions. Appl. Sci. Res., vol. 25, no. 3/4, Dec. 1971, pp. 201-214.
5. Englert, Gerald W.: Effect of Co-ordinate Space Phenomena on End Losses from, and Distributions Inside, Magnetic Mirror Systems. Nucl. Fusion, vol. 10, no. 4, Dec. 1970, pp. 361-368.
6. Englert, Gerald W.: Random Walk Theory of Charged Particles for Elastic and Inelastic Interactions. Ph.D. Thesis, Colorado State University, 1970.
7. Raether, H.: The Development of the Electron Avalanche in the Spark Canal. Zeit. f. Physik, vol. 112, 1939, pp. 464-489.
8. Schreider, Yu. A., ed.: Method of Statistical Testing, Monte Carlo Method. Elsevier Publ. Co., 1964.
9. Schmidt-Tiedemann, K. J.: Space Charge Retardation of Electron Avalanches. Zeit. f. Naturforsch., vol. 14A, Mar. 1959, pp. 989-994.
10. Heylen, A. E. D.: The Influence of Space Charge on the Spatial Development of an Electron Avalanche. Proceedings of Seventh International Conference on Phenomena in Ionized Gases. Vol. I. Gradevinska Knjega Publ. House, Beograd, 1965, pp. 563-565.
11. Raether, H.: The Effect of Eigen Space Charge of an Electron Avalanche on its Development. Comptes Rendus de la VI Conference Internationale sur les Phénomènes D'Ionisation dans les Gaz. Vol. 2. S.E.R.M.A., Paris, July 1963, pp. 305-307.
12. Crank, John: The Mathematics of Diffusion. Clarendon Press, 1956, p. 2.
13. Fletcher, R. C.: Impulse Breakdown in the 10^{-9} sec. Range of Air at Atmospheric Pressure. Phys. Rev., vol. 76, no. 10, Nov. 15, 1949, pp. 1501-1511.
14. Gradshteyn, I. S.; and Ryzhik, I. M.: Table of Integrals, Series, and Products. Fourth ed., A. Jeffrey, trans. ed., Academic Press, 1965.

NASA-Langley, 1973 —— 25 E-7074

NATIONAL AERONAUTICS AND SPACE ADMINISTRATION
WASHINGTON, D.C. 20546

OFFICIAL BUSINESS
PENALTY FOR PRIVATE USE $300

SPECIAL FOURTH-CLASS RATE
BOOK

POSTAGE AND FEES PAID
NATIONAL AERONAUTICS AND
SPACE ADMINISTRATION
451

U.S.MAIL

POSTMASTER: If Undeliverable (Section 158 Postal Manual) Do Not Return

"The aeronautical and space activities of the United States shall be conducted so as to contribute . . . to the expansion of human knowledge of phenomena in the atmosphere and space. The Administration shall provide for the widest practicable and appropriate dissemination of information concerning its activities and the results thereof."

—NATIONAL AERONAUTICS AND SPACE ACT OF 1958

NASA SCIENTIFIC AND TECHNICAL PUBLICATIONS

TECHNICAL REPORTS: Scientific and technical information considered important, complete, and a lasting contribution to existing knowledge.

TECHNICAL NOTES: Information less broad in scope but nevertheless of importance as a contribution to existing knowledge.

TECHNICAL MEMORANDUMS: Information receiving limited distribution because of preliminary data, security classification, or other reasons. Also includes conference proceedings with either limited or unlimited distribution.

CONTRACTOR REPORTS: Scientific and technical information generated under a NASA contract or grant and considered an important contribution to existing knowledge.

TECHNICAL TRANSLATIONS: Information published in a foreign language considered to merit NASA distribution in English.

SPECIAL PUBLICATIONS: Information derived from or of value to NASA activities. Publications include final reports of major projects, monographs, data compilations, handbooks, sourcebooks, and special bibliographies.

TECHNOLOGY UTILIZATION PUBLICATIONS: Information on technology used by NASA that may be of particular interest in commercial and other non-aerospace applications. Publications include Tech Briefs, Technology Utilization Reports and Technology Surveys.

Details on the availability of these publications may be obtained from:

SCIENTIFIC AND TECHNICAL INFORMATION OFFICE

NATIONAL AERONAUTICS AND SPACE ADMINISTRATION

Washington, D.C. 20546